Planetary Dynamos

F. H. Busse[1] and R. Simitev[2]
[1] *Physikalisches Institut der Universität Bayreuth, D-95440 Bayreuth, Germany*
[2] *Department of Mathematics, University of Glasgow, Glasgow G12 8QW, UK*
email: busse@uni-bayreuth.de
(Dated: December 28, 2012)

The theory of planetary dynamos and its applications to observed phenomena of planetary magnetism are outlined. It is generally accepted that convection flows driven by thermal or compositional buoyancy are the most likely source for the sustenance of global planetary magnetic fields. While the existence of dynamos in electrically conducting fluid planetary cores provides constraints on properties of the latter, the lack of knowledge about time dependences of the magnetic fields and about their toroidal components together with the restricted parameter regions accessible to theory have prevented so far a full understanding of the phenomena of planetary magnetism.

PACS numbers:

1. HISTORICAL INTRODUCTION

While the Earth's magnetism has been studied for centuries starting with the first scientific monograph of Gilbert (1600), the question of the magnetism of other planets had received scant attention until recently because of the lack of relevant observations. Only in 1955 clear evidence for the existence of a planetary magnetic field other than the geomagnetic one was obtained through the observation of the Jovian decametric radio waves (Burke and Franklin, 1955). Since it had been more or less accepted until the end of the 19-th century that geomagnetism arises from the remnant magnetization of the Earth similar properties may have been assumed for the other terrestrial planets and the Moon. This view lost its appeal, however, when it became evident that the Curie-temperature is exceeded in the Earth below a depth of about 30 km. Ferromagnetic materials in the Earth's crust could thus explain only magnetic fields with a relatively short wavelength.

The current period of intense research on the magnetism of planets other than that of the Earth started with the first detailed measurement of Jupiter's magnetic field by the Pioneer 10 space probe in 1973 and the discovery of Mercury's magnetism by Mariner 10 in 1974. In the early seventies also the development of the theory of magnetohydrodynamic dynamos had started in which the reaction of the Lorentz force of the generated magnetic field is taken into account in physically realistic configurations (Childress and Soward, 1972; Busse, 1973; Soward, 1974). Until that time dynamo theoreticians had focused their attention on the kinematic problem in which the possibility of growing magnetic fields driven by somewhat arbitrarily chosen velocity fields is considered. It must be remembered that only a few years earlier it had been demonstrated by Backus (1958) and Herzenberg (1958) in a mathematically convincing way that the homogeneous dynamo process of the generation of magnetic fields in a singly connected domain of an electrically conducting fluid is indeed possible. Doubts about the feasibility of this process which had first been proposed by Larmor (1919) had persisted after Cowling (1934) had proved that purely axisymmetric fields could not be generated in this way.

The complexity of the magnetohydrodynamic dynamo problem described by the nonlinearly coupled Navier-Stokes equations and the equation of magnetic induction had prevented progress in understanding planetary dynamos through analytical solutions. Only the advent of powerful enough computers in the 1990-ies has allowed to solve numerically the coupled three-dimensional partial differential equations through forward integration in time. Even today and for the foreseeable future the limits of computer capacity will permit the exploration of only a small fraction of the parameter space of interest for the understanding of planetary dynamos.

In view of the difficulties of a rigorous theory of planetary dynamos, many attempts have been made to obtain simple similarity relationships which would fit the observed planetary magnetic moments as function of certain properties of the planets. Some early proponents have gone as far as claiming the existence of a "magnetic Bode's law" corresponding to a relationship between the magnetic moment and size or angular momentum of a planet in analogy to the Titius-Bode law for the radii of the orbits of the planets. Just as in the latter case, however, attempts to derive a magnetic Bode's law from basic physical principles have failed.

Other proposals have taken into account physical forces. Since a common ingredient of planetary dynamos is the existence of a fluid part of the core with a sufficiently high electrical conductivity the latter parameter together with the core radius and the angular velocity of the planetary rotation usually enter the similarity relationships such as those proposed by Hide (1974), Busse (1976), Jacobs (1979) and Dolginov (1977). Malkus (1968, 1996) has argued for the precession of the Earth as the cause of geomagnetism and he and Vanyo (1984)

have demonstrated through laboratory experiments that precession and tides may cause turbulent motions in fluid planetary cores. Dolginov (1977) proposed a scaling law for the precessional origin of all planetary magnetic fields. While a dynamo driven by turbulent flows caused by precession and tides can not be easily excluded in the case of the Earth (Tilgner, 2005), it is much less likely in the case of other planets such as Uranus for which precessional torques are rather minute. Just as a common precessional origin of planetary magnetism is not regarded as feasible, so have all other proposed similarity relationships lost in appeal and are no longer seriously considered. We shall return, however, to scaling relationships based more directly on the basic equations in section 6.

2. GENERAL REMARKS ON THE DYNAMO THEORY OF PLANETARY MAGNETISM

Since the proposal of the geodynamo as the cause of the Earth's magnetism had been in doubt for a long time before 1958, numerous alternative proposals had been made in the literature. Among these only the possibility that thermoelectric currents may generate a planetary magnetic field is still discussed in the case of Mercury (Stevenson, 1987; Giampieri and Balogh, 2002). For a discussion of the failings of the various proposals for non-dynamo origins of planetary magnetic fields we refer to the papers of Bullard (1949) and Stevenson (1983). Although the dynamo hypothesis of the origin of planetary magnetism is not without difficulties, it is the only one considered seriously at the present time with the possible exception of the just mentioned case of Mercury.

Dynamos generally convert mechanical energy into magnetic one. In contrast to the technical dynamo which is characterized by a multiply connected region of high electrical conductivity, i.e. it depends on an appropriate wiring, planetary dynamos are referred to as homogeneous dynamos since they operate in a singly connected domain of high electrical conductivity. Since flows in planetary cores with active dynamos are usually turbulent the small scale structure of the magnetic field is correspondingly chaotic. The large scale structure, however, can be quite regular. One distinguishes "steady" and oscillatory dynamos. The most famous example of the latter kind is the solar dynamo which exhibits a well defined period of about 22 years. The geodynamo, on the other hand, is a "steady" dynamo, even though it varies in its amplitude by a factor of two or more on the magnetic diffusion time scale and reverses its polarity on a longer time scale. A measure of the magnetic diffusion time is given by the decay time, $t_d = \sigma\mu r_0^2/\pi^2$, of the magnetic field in the absence of fluid motions. Here σ and μ refer to the electrical conductivity and the magnetic permeability of the planetary core of radius r_0. In the case of the Earth the decay time is of the order of 20 000 years, but it may vary between a few hundred and a million years for other examples of planetary dynamos.

The theory of homogeneous dynamos is based on Maxwell's equations for the magnetic flux density $\boldsymbol{B}$, the electric current density $\boldsymbol{j}$ and the electric field $\boldsymbol{E}$ in the magnetohydrodynamic approximation in which the displacement current is neglected. This approximation is highly accurate as long as the fluid velocity is small compared to the velocity of light which is certainly the case for all planetary applications. These equations together with Ohm's law for a moving conductor are given by

$$\nabla \cdot \boldsymbol{B} = 0, \qquad \frac{\partial}{\partial t}\boldsymbol{B} = -\nabla \times \boldsymbol{E}, \tag{1a}$$

$$\nabla \times \boldsymbol{B} = \mu \boldsymbol{j}, \qquad \boldsymbol{j} = \sigma(\boldsymbol{v} \times \boldsymbol{B} + \boldsymbol{E}), \tag{1b}$$

where μ is the magnetic permeability of the fluid and σ is its electrical conductivity. These "pre-Maxwell" equations have the property that they are invariant with respect to a Galilei transformation, i. e. the equations remain unchanged in a new frame of reference moving with the constant velocity vector $\boldsymbol{V}$ relative to the original frame of reference. Indicating the variables of the new frame by a prime we find

$$\boldsymbol{v}' = \boldsymbol{v} - \boldsymbol{V}, \qquad \frac{\partial}{\partial t'} = \frac{\partial}{\partial t} + \boldsymbol{V} \cdot \nabla, \tag{2a}$$

$$\boldsymbol{B}' = \boldsymbol{B}, \qquad \boldsymbol{E}' = \boldsymbol{E} + \boldsymbol{V} \times \boldsymbol{B}, \qquad \boldsymbol{j}' = \boldsymbol{j}\ . \tag{2b}$$

This invariance is the basis for the combination in MHD of equations (1) with the equations of hydrodynamics in their usual non-relativistic form. It is remarkable that this invariance does not only hold with respect to a Galilei transformation, but with respect to a transformation to a rotating frame of reference as well. In that case $\boldsymbol{V}$ is replaced by $\boldsymbol{\Omega} \times \boldsymbol{r}$ in equations (2), but when $\frac{\partial}{\partial t'}$ is operating on any vector $\boldsymbol{a}$ the term $-\boldsymbol{\Omega} \times \boldsymbol{a}$ must be added on the right hand side, since even a constant vector field becomes time dependent when seen from a rotating frame unless it is parallel to $\boldsymbol{\Omega}$.

Elimination of $\boldsymbol{E}$ and $\boldsymbol{j}$ from equation (1) yields the equation of magnetic induction

$$\nabla \times \left(\frac{1}{\sigma\mu} \nabla \times \boldsymbol{B} \right) = \frac{\partial}{\partial t}\boldsymbol{B} + \nabla \times (\boldsymbol{v} \times \boldsymbol{B}) \tag{3}$$

which for a solenoidal velocity field $\boldsymbol{v}$ and a constant magnetic diffusivity $\lambda \equiv (\sigma\mu)^{-1}$ can be further simplified,

$$\left(\frac{\partial}{\partial t} + \boldsymbol{v} \cdot \nabla \right) \boldsymbol{B} - \lambda \nabla^2 \boldsymbol{B} = \boldsymbol{B} \cdot \nabla \boldsymbol{v}. \tag{4}$$

This equation has the form of a heat equation with the magnetic field line stretching term on the right hand side acting as a heat source. This interpretation is especially useful for the dynamo problem. In order that a magnetic field $\boldsymbol{B}$ may grow, the term on the right hand side of (4) must overcome the effect of the magnetic diffusion term

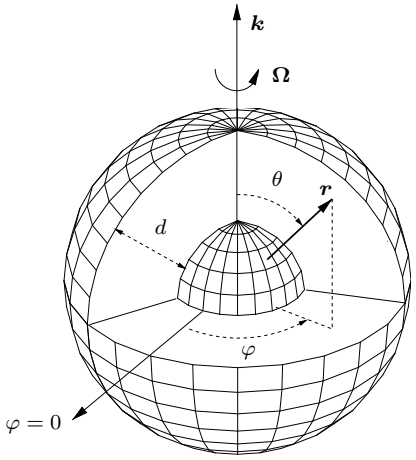

FIG. 1: *Geometrical configuration of the problem. A part of the outer spherical surface is removed to expose the interior of the shell to which the conducting fluid is confined.*

on the left hand side. Using a typical velocity U and a typical length scale d, the ratio of the two terms can be estimated by the magnetic Reynolds number Rm,

$$Ud/\lambda \equiv Rm. \tag{5}$$

Only when Rm is of the order one or larger may growing magnetic fields become possible.

In the following we shall first consider the mathematical formulation of the problem of convection driven dynamos in rotating spherical shells in a simple form in which only the physically most relevant parameters are taken into account. Before discussing dynamo solutions in section 5 we shall briefly outline in section 4 properties of convection it the absence of a magnetic field. Applications to various planets and moons will be considered in section 6 of this article and some concluding remarks are given in section 7.

3. MATHEMATICAL FORMULATION OF THE PROBLEM OF SPHERICAL DYNAMOS

A sketch of the geometrical configuration that will be considered is shown in figure 1. For the equations describing convection driven dynamos in the frame rotating with the angular velocity Ω we use a standard formulation which has also been used for a dynamo benchmark (Christensen *et al.* 2001). But we assume different scales and assume that a more general static state exists with the temperature distribution $T_S = T_0 - \beta d^2 r^2/2 + \Delta T \eta r^{-1}(1-\eta)^{-2}$ where η denotes the ratio of inner to outer radius of the spherical shell and d is its thickness. ΔT is the temperature difference between the boundaries in the special case $\beta = 0$. In the case $\Delta T = 0$ the static temperature distribution T_S corresponds to that of a homogeneously heated sphere with the heat source density proportional to the parameter β. The gravity field is given by $\boldsymbol{g} = -\gamma d \boldsymbol{r}$ where $\boldsymbol{r}$ is the position vector with respect to the center of the sphere and r is its length measured in units of d.

In addition to d, the time d^2/ν, the temperature $\nu^2/\gamma\alpha d^4$ and the magnetic flux density $\nu(\mu\varrho)^{1/2}/d$ are used as scales for the dimensionless description of the problem where ν denotes the kinematic viscosity of the fluid, κ its thermal diffusivity and ϱ its density. The Boussinesq approximation is used in that ϱ is assumed to be constant except in the gravity term where its temperature dependence given by $\alpha \equiv -(d\varrho/dT)/\varrho = \text{const.}$ is taken into account. The dimensionless equations of motion, the heat equation for the deviation Θ of the temperature field from the static distribution and the equation of magnetic induction thus assume the form

$$\nabla^2 \boldsymbol{v} + \boldsymbol{B}\cdot\nabla\boldsymbol{B} + \boldsymbol{r}\Theta - \nabla\pi = P^{-1}(\partial_t \boldsymbol{v} + \boldsymbol{v}\cdot\nabla\boldsymbol{v}) + \tau \mathbf{k}\times\boldsymbol{v} \tag{6a}$$

$$\nabla\cdot\boldsymbol{v} = 0 \tag{6b}$$

$$\nabla^2\Theta + \left[R_i + R_e\eta r^{-3}(1-\eta)^{-2}\right]\boldsymbol{r}\cdot\boldsymbol{v} = P(\partial_t + \boldsymbol{v}\cdot\nabla)\Theta \tag{6c}$$

$$P_m\left(\frac{\partial}{\partial t} + \boldsymbol{v}\cdot\nabla\right)\boldsymbol{B} - \nabla^2\boldsymbol{B} = P_m\boldsymbol{B}\cdot\nabla\boldsymbol{v} \tag{6d}$$

where $\mathbf{k}$ is the unit vector in the direction of the axis of rotation and where $\nabla\pi$ includes all terms that can be written as gradients. The Rayleigh numbers R_i and R_e, the Coriolis parameter τ, the Prandtl number P and the magnetic Prandtl number P_m are defined by

$$R_i = \frac{\alpha\gamma\beta d^6}{\nu\kappa},\quad R_e = \frac{\alpha\gamma\Delta T d^4}{\nu\kappa}, \tag{7a}$$

$$\tau = \frac{2\Omega d^2}{\nu},\quad P = \frac{\nu}{\kappa},\quad P_m = \frac{\nu}{\lambda} \tag{7b}$$

For simplicity $R_e = 0$ will be assumed unless indicated otherwise. The notation $R \equiv R_i$ will thus be used in the following. The Prandtl number P has been added as an important parameter of the problem even though $P = 1$ is often assumed with the argument that all effective diffusivities are equal in turbulent media. The effective diffusivities of scalar and vector quantities in turbulent fluid flow differ in general, however, and large differences in the corresponding molecular diffusivities will not be erased entirely in the turbulent case.

Since the velocity field $\boldsymbol{v}$ as well as the magnetic flux density $\boldsymbol{B}$ are solenoidal vector fields, the general representation in terms of poloidal and toroidal components can be used,

$$\boldsymbol{v} = \nabla\times(\nabla\Phi\times\boldsymbol{r}) + \nabla\Psi\times\boldsymbol{r}\ , \tag{8a}$$

$$\boldsymbol{B} = \nabla\times(\nabla h\times\boldsymbol{r}) + \nabla g\times\boldsymbol{r}\ . \tag{8b}$$

By multiplying the $(\text{curl})^2$ and the curl of equation (6a)

by $\boldsymbol{r}$ we obtain two equations for Φ and Ψ

$$[(\nabla^2 - \partial_t)L_2 + \tau\partial_\phi]\nabla^2\Phi + \tau Q\Psi - L_2\Theta = -\boldsymbol{r}\cdot\nabla\times[\nabla\times(\boldsymbol{v}\cdot\nabla\boldsymbol{v} - \boldsymbol{B}\cdot\nabla\boldsymbol{B})] \quad (9a)$$

$$[(\nabla^2 - \partial_t)L_2 + \tau\partial_\phi]\Psi - \tau Q\Phi = \boldsymbol{r}\cdot\nabla\times(\boldsymbol{v}\cdot\nabla\boldsymbol{v} - \boldsymbol{B}\cdot\nabla\boldsymbol{B}) \quad (9b)$$

where ∂_t and ∂_ϕ denote the partial derivatives with respect to time t and with respect to the angle ϕ of a spherical system of coordinates r, θ, ϕ and where the operators L_2 and Q are defined by

$$L_2 \equiv -r^2\nabla^2 + \partial_r(r^2\partial_r)$$

$$Q \equiv r\cos\theta\nabla^2 - (L_2 + r\partial_r)(\cos\theta\partial_r - r^{-1}\sin\theta\partial_\theta)$$

The equations for h and g are obtained through the multiplication of equation (6d) and of its curl by $\boldsymbol{r}$,

$$\nabla^2 L_2 h = P_m[\partial_t L_2 h - \boldsymbol{r}\cdot\nabla\times(\boldsymbol{v}\times\boldsymbol{B})] \quad (10a)$$

$$\nabla^2 L_2 g = P_m[\partial_t L_2 g - \boldsymbol{r}\cdot\nabla\times(\nabla\times(\boldsymbol{v}\times\boldsymbol{B}))] \quad (10b)$$

Either rigid boundaries with fixed temperatures as in the benchmark case (Christensen *et al.* 2001),

$$\Phi = \partial_r(r\Phi) = \Psi = \Theta = 0 \quad \text{at} \quad r = r_i \equiv \eta/(1-\eta)$$

$$\text{and at} \quad r = r_o = (1-\eta)^{-1}, \quad (11)$$

or stress-free boundaries with fixed temperatures,

$$\Phi = \partial^2_{rr}\Phi = \partial_r(\Psi/r) = \Theta = 0 \quad \text{at} \quad r = r_i \equiv \eta/(1-\eta)$$

$$\text{and at} \quad r = r_o = (1-\eta)^{-1} \quad (12)$$

are often used. The latter boundary conditions are assumed in the following since they allow to cover numerically a larger region of the parameter space. The case $\eta = 0.4$ will be considered unless indicated otherwise. It provides a good compromise for the study of both, the regions inside and outside the tangent cylinder. The latter is the cylindrical surface touching the inner spherical boundary at its equator. For the magnetic field electrically insulating boundaries are used such that the poloidal function h must be matched to the function $h^{(e)}$ which describes the potential fields outside the fluid shell

$$g = h - h^{(e)} = \partial_r(h - h^{(e)}) = 0 \ \text{ at } r = r_i \text{ and } r = r_o. \quad (13)$$

But computations for the case of an inner boundary with no-slip conditions and an electrical conductivity equal to that of the fluid have also been done. The numerical integration of equations (2) together with boundary conditions (4) proceeds with the pseudo-spectral method as described by Tilgner and Busse (1997) and Tilgner (1999)

E	Average density of kinetic energy	(18)
E_p, E_t	Energy densities of poloidal and toroidal components of motion	(18)
η	Radius ratio of fluid shell	
Λ	Elsasser number	(20)
M	Average magnetic energy density	(19)
M_p, M_t	Energy densities of poloidal and toroidal components of the magnetic field	(19)
Nu	Nusselt number	(16)
P	Prandtl number	(7b)
P_m	Magnetic Prandtl number	(7b)
R	Rayleigh number	(7a)
R_c	Critical value of R for onset of convection	
Rm	Magnetic Reynolds number $= P_m\sqrt{2E}$	
τ	Coriolis parameter	(7a)

TABLE I: *Important dimensionless parameters.*

which is based on an expansion of all dependent variables in spherical harmonics for the θ, ϕ-dependences, i.e.

$$\Phi = \sum_{l,m} V_l^m(r,t)P_l^m(\cos\theta)\exp\{im\phi\} \quad (14)$$

and analogous expressions for the other variables, Ψ, Θ, h and g. P_l^m denotes the associated Legendre functions. For the r-dependence expansions in Chebychev polynomials are used.

For the computations to be reported in the following a minimum of 33 collocation points in the radial direction and spherical harmonics up to the order 64 have been used. But in many cases the resolution was increased to 49 collocation points and spherical harmonics up to the order 96 or 128.

It should be emphasized that the static state $\boldsymbol{v} = \boldsymbol{B} = \Theta = 0$ represents a solution of equations (6) for all values of the Rayleigh numbers R_i and R_e, but this solution is unstable except for low or negative values of the latter parameters. Similarly, there exist solutions with $\boldsymbol{B} = 0$, but $\boldsymbol{v} \neq 0, \Theta \neq 0$, for sufficiently large values of either R_i or R_e or both, but, again, these solutions are unstable for sufficiently large values of P_m with respect to disturbances with $\boldsymbol{B} \neq 0$. Dynamo solutions as all solutions with $\boldsymbol{B} \neq 0$ are called are thus removed by at least two bifurcations from the basic static solution of the problem.

Finally we present in table 1 a list of the most important parameters used in the following sections.

4. CONVECTION IN ROTATING SPHERICAL SHELLS

For an introduction to the problem of convection in spherical shells we refer to the review of Busse (2002a).

Convection tends to set in first outside the tangent cylinder in the form of thermal Rossby waves for which the Coriolis force is balanced almost entirely by the pressure gradient. The model of the rotating cylindrical annulus has been especially useful for the understanding of this type of convection. A rough idea of the dependence of the critical Rayleigh number R_c for the onset of convection on the parameters of the problem can be gained from the expressions derived from the annulus model (Busse, 1970)

$$R_c = 3\left(\frac{P\tau}{1+P}\right)^{\frac{4}{3}} (\tan\theta_m)^{\frac{8}{3}} r_m^{-\frac{1}{3}} 2^{-\frac{2}{3}} \qquad (15a)$$

$$m_c = \left(\frac{P\tau}{1+P}\right)^{\frac{1}{3}} (r_m \tan\theta_m)^{\frac{2}{3}} 2^{-\frac{1}{6}} \qquad (15b)$$

$$\omega_c = \left(\frac{\tau^2}{(1+P)^2 P}\right)^{\frac{1}{3}} 2^{-\frac{5}{6}} (\tan^2\theta_m / r_m)^{\frac{2}{3}} \qquad (15c)$$

where r_m refers to the mean radius of the fluid shell, $r_m = (r_i + r_o)/2$, and θ_m to the corresponding colatitude, $\theta_m = \arcsin(r_m(1-\eta))$. The azimuthal wavenumber of the preferred mode is denoted by m_c and the corresponding angular velocity of the drift of the convection columns in the prograde direction is given by ω_c/m_c.

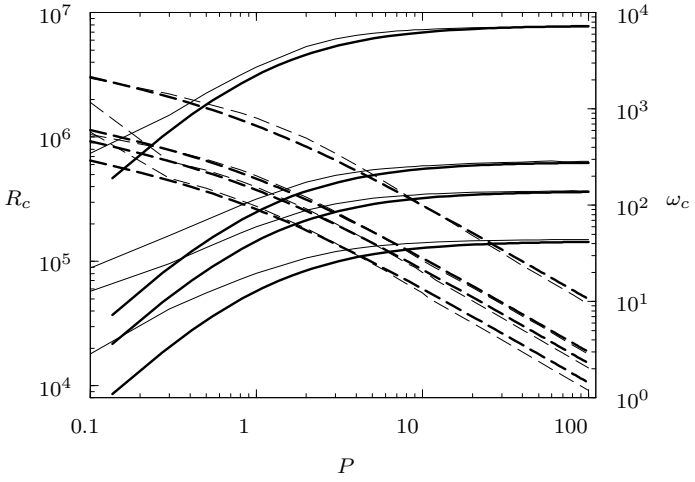

FIG. 2: *Critical Rayleigh number R_c (thin solid lines) and frequency ω_c (right ordinate, thin dashed lines) as a function of the Prandtl number P in the case $\eta = 0.4$ for the Coriolis numbers $\tau = 5\times10^3$, 10^4, 1.5×10^4 and 10^5 (from bottom to top). The thick lines correspond to expressions (15a) and (15c).*

In figure 2 expressions (15a,c) are compared with accurate numerical values which indicate that the general trend is well represented by expressions (15a,c). The same property holds for m_c. For a rigorous asymptotic analysis in the case $P = 1$ including the radial dependence we refer to Jones *et al.* (2000).

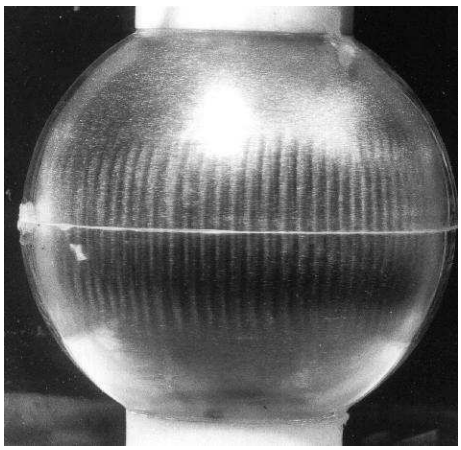

FIG. 3: *Banana cells in a thin rotating spherical fluid shell cooled from within. Convection driven by centrifugal buoyancy is made visible by a suspension of tiny flakes which become aligned with the shear. (After Busse and Carrigan, 1976)*

It is evident from figure 2 that the agreement between expressions (15) and the numerical values deteriorates as low values of P are approached. This behavior is caused by the fact that instead of the thermal Rossby wave mode the inertial mode of convection becomes preferred at onset for sufficiently low Prandtl numbers. It is characterized by convection cells attached to the equatorial region of the outer boundary not unlike the "banana cells" seen in the narrow gap experiment of figure 3 . The equatorially attached convection does indeed represent an inertial wave modified by the effects of viscous dissipation and thermal buoyancy. An analytical description of this type of convection can thus be attained through the introduction of viscous friction and buoyancy as perturbations as has been done by Zhang(1994) and by Busse and Simitev (2004) for stress-free and by Zhang (1995) for no-slip boundaries. According to Ardes *et al.* (1997) equatorially attached convection is preferred at onset for $\tau < \tau_l$ where τ_l increases in proportion to $P^{-1/2}$.

A third form of convection is realized in the polar regions of the shell which comprise the two fluid domains inside the tangent cylinder. Since gravity and rotation vectors are nearly parallel in these regions (unless values of η close to unity are used) convection resembles the kind realized in a horizontal layer heated from below and rotating about a vertical axis. Because the Coriolis force can not be balanced by the pressure gradient in this case, the onset of convection is delayed to higher values of R where convection outside the tangent cylinder has reached already high amplitudes. In the case of $\eta = 0.4$ the onset of convection in the polar regions typically occurs at Rayleigh numbers which exceed the critical values R_c for onset of convection outside the tangent cylinder by a factor of the order 4. Except for the case of very

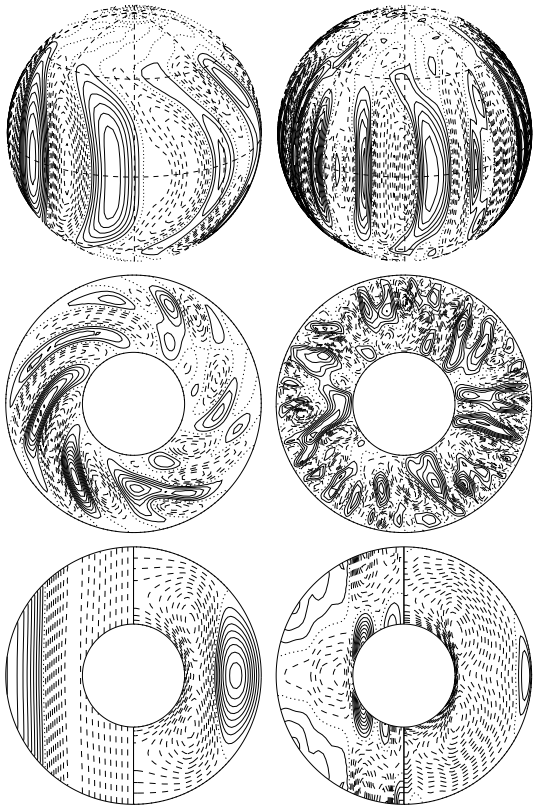

FIG. 4: *Convection in rotating spherical fluid shells in the cases $\tau = 10^4$, $R = 4 \times 10^5$, $P = 1$ (left column) and $\tau = 5 \times 10^3$, $R = 8 \times 10^5$, $P = 20$ (right column). Lines of constant u_r in the middle spherical surface, $r = r_i + 0.5$ are shown in the upper row. The plots of the middle row show streamlines, $r\partial\Phi/\partial\varphi = const.$, in the equatorial plane. The lowermost plots indicate lines of constant mean azimuthal velocity $\bar{u}_\varphi$ in the left halves and isotherms of $\bar{\Theta}$ in the right halves.*

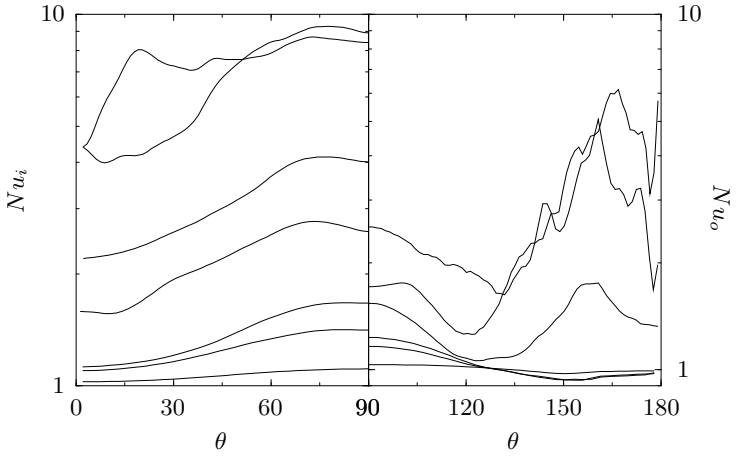

FIG. 5: *The time- and azimuthally-averaged local Nusselt numbers at the inner spherical boundary Nu_i (left plot) and at the outer spherical boundary Nu_o (right plot) as functions of the colatitude θ for $P = 0.5$, $\tau = 1.5 \times 10^4$ and $R = 4, 8, 10, 15, 20, 30, 25 \times 10^5$ (from bottom to top at 90°).*

low Prandtl numbers the retrograde differential rotation in the polar regions generated by convection outside the tangent cylinder tends to facilitate polar convection by reducing the rotational constraint. A tendency towards an alignment of convection rolls with the North-South direction (Busse and Cuong 1977) can be noticed, but this property is superseded by instabilities of the Küppers-Lortz type (for an experimental demonstration see Busse and Heikes (1980)) and by interactions with turbulent convection outside the tangent cylinder.

Typical features of low and high Prandtl number convection are illustrated in figure 4. The columnar nature of convection does not vary much with P as is evident from the top two plots of the figure. At Prandtl numbers of the order unity or less, - but not in the case of inertial convection-, the convection columns tend to spiral away from the axis and thereby create a Reynolds stress which drives a strong geostrophic differential rotation as shown in the bottom left plot of the figure. This differential rotation in turn promotes the tilt and a feedback loop is thus created. At high values of P the Reynolds stress becomes negligible and no significant tilt of the convection columns is apparent. In this case the differential rotation is generated in the form of a thermal wind caused by the latitudinal gradient of the axisymmetric component of Θ.

Among the properties of convection at finite amplitudes the heat transport is the most important one. Customarily its efficiency is measured by the Nusselt number which is defined as the heat transport in the presence of convection divided by the heat transport in the absence of motion. In the case of the spherical fluid shell two Nusselt numbers can be defined measuring the efficiency of convection at the inner and the outer boundary,

$$Nu_i = 1 - \frac{P}{r_i} \left. \frac{d\overline{\overline{\Theta}}}{dr} \right|_{r=r_i} \qquad Nu_o = 1 - \frac{P}{r_o} \left. \frac{d\overline{\overline{\Theta}}}{dr} \right|_{r=r_o} \tag{16}$$

where the double bar indicates the average over the spherical surface. In addition local Nusselt numbers

$$Nu_i(\theta) = 1 - \frac{P}{r_i} \left. \frac{d\overline{\Theta}}{dr} \right|_{r=r_i} \qquad Nu_o(\theta) = 1 - \frac{P}{r_o} \left. \frac{d\overline{\Theta}}{dr} \right|_{r=r_o} \tag{17}$$

are of interest where only the azimuthal average is applied, as indicated by the single bar, instead of the average over the entire spherical surface. Examples of such measures of the dependence of the heat transport on latitude are shown in figure 5. This figure demonstrates that at low supercritical Rayleigh numbers the heat transport occurs primarily across the equatorial region, but as R increases the heat transport in the polar regions takes

off and soon exceeds that at low latitudes. This process is especially evident at the outer boundary. In the polar regions convection is better adjusted for carrying heat from the lower boundary to the upper one, and it is known from computations of the convective heat transport in horizontal layers rotating about a vertical axis that the value of Nu may exceed the value in a non-rotating layer at a given value of R in spite of the higher critical Rayleigh number in the former case (Somerville and Lipps, 1973).

Outside the tangent cylinder the convective heat transport encounters unfavorable conditions in that the cylindrical form of the convection eddies is not well adjusted to the spherical boundaries. This handicap is partly overcome through the onset of time dependence in the form of vacillations in which the convection columns expand and contract in the radial direction or vary in amplitude.

At Prandtl numbers of the order unity and less another effect restricts the heat transport. The shear of the geostrophic differential rotation created by the Reynolds stresses of the convection columns severely inhibits the heat transport. To illustrate this effect we have plotted in figure 6 in addition to the Nusselt numbers the averages of the kinetic energy densities of the various components of the convection flow which are defined by

$$\overline{E}_p = \frac{1}{2}\langle \mid \nabla \times (\nabla \bar{\Phi} \times \boldsymbol{r}) \mid^2 \rangle, \quad \overline{E}_t = \frac{1}{2}\langle \mid \nabla \bar{\Psi} \times \boldsymbol{r} \mid^2 \rangle, \tag{18a}$$

$$\check{E}_p = \frac{1}{2}\langle \mid \nabla \times (\nabla \check{\Phi} \times \boldsymbol{r}) \mid^2 \rangle, \quad \check{E}_t = \frac{1}{2}\langle \mid \nabla \check{\Psi} \times \boldsymbol{r} \mid^2 \rangle, \tag{18b}$$

where the angular brackets indicate the average over the fluid shell and $\bar{\Phi}$ refers to the azimuthally averaged component of Φ, while $\check{\Phi}$ is defined by $\check{\Phi} = \Phi - \bar{\Phi}$. Analogous definitions hold for the energy densities of the magnetic field,

$$\overline{M}_p = \frac{1}{2}\langle \mid \nabla \times (\nabla \bar{h} \times \boldsymbol{r}) \mid^2 \rangle, \quad \overline{M}_t = \frac{1}{2}\langle \mid \nabla \bar{g} \times \boldsymbol{r} \mid^2 \rangle, \tag{19a}$$

$$\check{M}_p = \frac{1}{2}\langle \mid \nabla \times (\nabla \check{h} \times \boldsymbol{r}) \mid^2 \rangle, \quad \check{M}_t = \frac{1}{2}\langle \mid \nabla \check{g} \times \boldsymbol{r} \mid^2 \rangle. \tag{19b}$$

The total magnetic energy density M averaged over the fluid shell is thus given by $M = \overline{M}_p + \overline{M}_t + \check{M}_p + \check{M}_t$.

Figure 6 is instructive in that it demonstrates both, convection in the presence and in the absence of its dynamo generated magnetic field. As is evident from the right part of figure 6 with $M \sim 0$ relaxation oscillations occur in which convection sets in nearly periodically for short episodes once the energy $\overline{E}_t$ of the differential rotation has decayed to a sufficiently low amplitude. But as soon as convection grows in amplitude, the differential rotation grows as well and shears off the convection

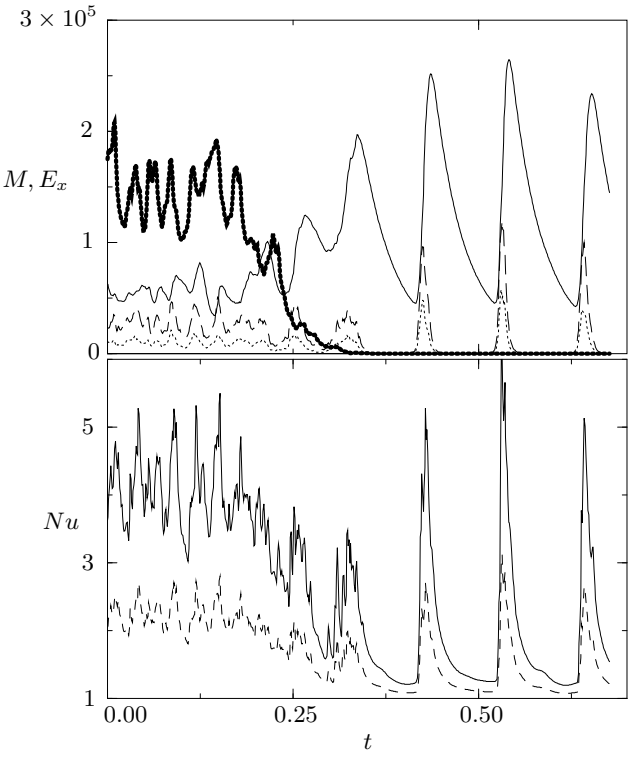

FIG. 6: *Decay of a dynamo for $P = 0.5$, $\tau = 1.5 \times 10^4$, $R = 1.2 \times 10^6$, $P_m = 0.5$. The total magnetic energy density M (thick dotted line, multiplied by a factor of 5), the kinetic energy densities $\overline{E}_t$ (solid line), $\check{E}_p$ (dotted line), $\check{E}_t$ (dashed line), and Nusselt numbers Nu_i (solid line) at the inner and Nu_o (dashed line) at the outer spherical boundary (lower plot) are plotted as functions of time t.*

columns. After convection has stopped the differential rotation decays on the viscous time scale until the process repeats itself.

As long as the magnetic field is present $\overline{E}_t$ is suppressed owing to the action of the Lorentz force and high Nusselt numbers are obtained. The dynamo generated magnetic field thus acts in a fashion quite different from that of a homogeneous field which typically counteracts the effects of rotation and tends to minimize the critical value of the Rayleigh number when the Elsasser number,

$$\Lambda = \frac{2MP_m}{\tau} \tag{20}$$

assumes the value 1 in the case of a plane layer (Chandrasekhar 1961) or values of the same order in the case of a sphere (Fearn 1979) or in the related annulus problem (Busse 1983) .

5. CONVECTION DRIVEN DYNAMOS

It appears that dynamos are generated by convection in rotating spherical shells for all parameter values as

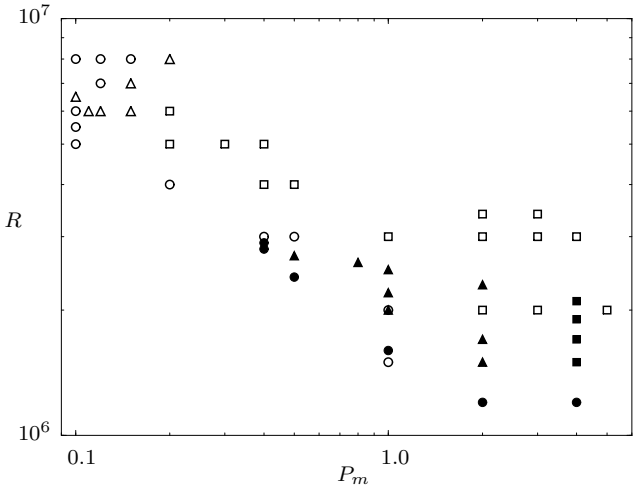

FIG. 7: *Convection driven dynamos as a function of the Rayleigh number R and the magnetic Prandtl number P_m for $P = 0.1$, $\tau = 10^5$ (empty symbols) and for $P = 1$, $\tau = 3 \times 10^4$ (filled symbols). The symbols indicate chaotic dipolar (squares), hemispherical (triangles), and decaying dynamos (circles).*

long as the magnetic Reynolds number is of the order 50 or higher and the fluid is not too turbulent. Since Rm can be defined by $P_m\sqrt{2E}$ where the kinetic energy density, $E = \overline{E}_p + \overline{E}_t + \check{E}_p + \check{E}_t$, increases with R, increasing values of the Rayleigh number are required for dynamos as P_m decreases. In planetary cores the latter parameter may assume values as low as 10^{-5} or 10^{-6}, but numerical simulation have achieved so far only values somewhat below 10^{-1}. The trend of increasing R with decreasing P_m is evident in figure 7 where results are shown for two different values of τ and P. It is also evident from the results in the upper left corner of the figure that an increasing R may be detrimental for dynamo action. This is a typical property of marginal dynamos at the boundary of dynamos in the parameter space (Christensen *et al.* 1999, Simitev and Busse 2005). Since convection at the relevant values of R is chaotic this property also holds for the generated magnetic field. The magnetic energy must be finite near the boundary of dynamos in the parameter space because a sufficient amplitude of the fluctuating components of the convection flow can be obtained only when the magnetic field is strong enough to suppress the differential rotation. This property appears to hold even at high Prandtl numbers where differential rotation occurs only in the form of a relatively weak thermal wind.

Even in its chaotic state convection at high values of τ exhibits a strong symmetry with respect to the equatorial plane at high values of τ, at least as long as convection in the polar regions is still weak. Because of this symmetry magnetic fields can be generated either with

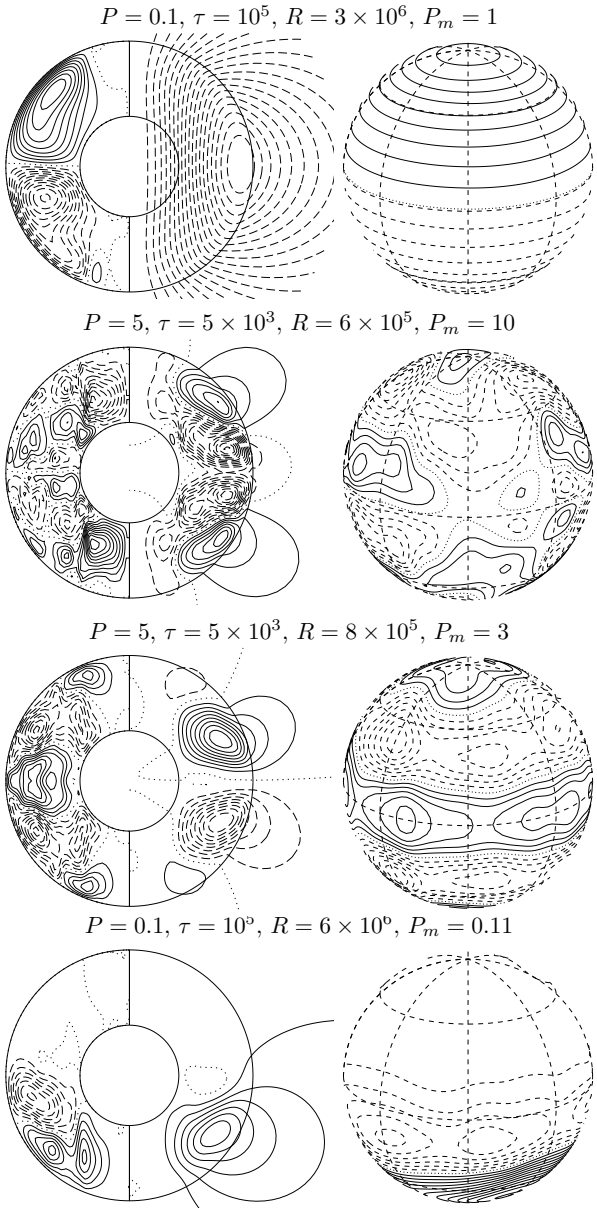

FIG. 8: *Various types of dynamo symmetry. The left column shows lines of $\overline{B}_\varphi = const.$ (left half) and $r \sin\theta \partial_\theta \overline{h} = const.$ (right half). The right column shows surfaces of $B_r = const.$ at $r = r_o + 0.7$.*

the same symmetry as the convection flow, i.e. h and g are antisymmetric with respect to equatorial plane in which case one speaks of a quadrupolar dynamo, or the magnetic field exhibits the opposite symmetry with symmetric functions h and g in which case one speaks of a dipolar dynamo. Of special interest are hemispherical dynamos (Grote and Busse 2001) in which case the fields of dipolar and quadrupolar symmetry have nearly the same amplitude such that they cancel each other either in the Northern or the Southern hemisphere. Examples of typical dynamos with different symmetries are shown

in figure 8. Here it is also evident that low P and high P dynamos differ in the structure of their mean toroidal fields. While their mean poloidal dipolar fields exhibit hardly any difference, the high P dynamo is characterized by strong polar azimuthal flux tubes which are missing in the low P case. The reason for this difference is that the radial gradient of the differential rotation in the polar regions is much stronger for high P than for low P.

As the Rayleigh number increases and polar convection becomes stronger the convection flow looses some of its equatorial symmetry and the magnetic field can no longer easily be classified. Usually the dipolar component becomes more dominant in cases of dynamos which started as either quadrupolar or hemispherical dynamos at lower values of R.

It should be emphasized that quadrupolar and hemispherical dynamos are usually oscillatory in that new azimuthal flux tubes of alternating sign emerge in the equatorial plane, move towards higher latitudes, while old flux tubes are dissipated in the polar region. There also exist dipolar dynamos which exhibit the same type of oscillations. They are typically found in the parameter space near the region where hemispherical dynamos occur. To illustrate the dynamo oscillations additional plots separated at equal distances in time before the corresponding plot in the lower three rows of figure 8 are shown in figure 9. The four plots in each case cover approximately half a period of oscillation. It must be realized, of course, that the oscillations are not strictly periodic since they occur in a turbulent system. In this respect they resemble the solar cycle with its 22 year period. Because the solar dynamo is believed to operate at the bottom of the solar convection the propagation of the dynamo wave is towards low latitudes on the sun. A remarkable feature of the dipole oscillation in figure 9 is that the polar flux tubes hardly change in time. The oscillation appears to be confined to the region outside the tangent cylinder. At a lower value of P_m the strong polar flux tubes even inhibit the oscillation of the mean poloidal field as shown in figure 10. This case has been called the "invisibly" oscillating dynamo since at some distance from the boundary of the spherical fluid shell the oscillation of the dynamo can hardly be noticed.

The relatively simple magnetic fields displayed in figures 8, 9, and 10 should not be regarded as representative for high values of the Rayleigh number when R exceeds its critical value R_c by an order of magnitude or more. In that case the equatorial symmetry has nearly disappeared owing to the dominant convection in the polar regions and non-axisymmetric components of the field tend to exceed axisymmetric ones as shown , for example, in figure 11. The strong growth with increasing Rm of the non-axisymmetric magnetic flux is also evident in figure 12 when energies corresponding to different values of P_m are compared.

An important question is the average strength of the magnetic field generated by the dynamo process in dependence on the parameters. Two concepts are often used in attempts to answer this question. In astrophysical situations the equipartition between magnetic and kinetic energy is used as a guide. While such a balance may hold locally as, for example, in the neighborhood of sunspots, it is not likely to be applicable to global planetary magnetic fields. In the Earth's core, for example, the magnetic energy density exceeds the kinetic one by a factor of the order of 10^3. The second concept is based on the property that an Elsasser number Λ of the order unity appears to correspond to optimal conditions for convection in rotating systems in the presence of an applied nearly uniform magnetic field. While this idea may be useful as a first rough estimate, the results of numerical dynamo simulations do not support this concept very well. The examples shown in figure 12 exhibit Λ-values differing by an order of magnitude and even larger variations have been reported by Simitev and Busse (2005) and by Christensen and Aubert (2005).

Another important feature demonstrated in figure 12 is the change in the structure of the magnetic field with increasing Prandtl number. While for $P = 5$ and lower values the mean poloidal field is small in comparison with the fluctuating components, this situation changes dramatically at about $P = 8$ for $\tau = 5 \cdot 10^3$ such that for higher P the mean poloidal field becomes dominant. Usually this field is dipolar. This change is associated with the transition from the geostrophic differential rotation generated by Reynolds stresses to the thermal wind type differential rotation caused by a latitudinal temperature gradient. While the magnetic energy M may exceed the total kinetic energy E by orders of magnitude in particular for high Prandtl numbers, ohmic dissipation is usually found to be at most comparable to viscous dissipation in numerical simulations. But this may be due to the limited numerically accessible parameter space.

The brief introduction of this section to convection driven dynamos in rotating spherical fluid shells can only give an vague impression of the potential of numerical simulations for the understanding of planetary magnetism. Many more examples of such simulations can be found in the literature. Usually they have been motivated by applications to the geodynamo and $P = 1$ is assumed in most cases for simplicity. For some recent systematic investigations we refer to Christensen et al. (1999), Grote et al. (2000), Jones (2000), Grote and Busse (2001), Kutzner and Christensen (2000, 2002), Busse et al. (2003), Simitev and Busse (2005) and other papers referred to therein.

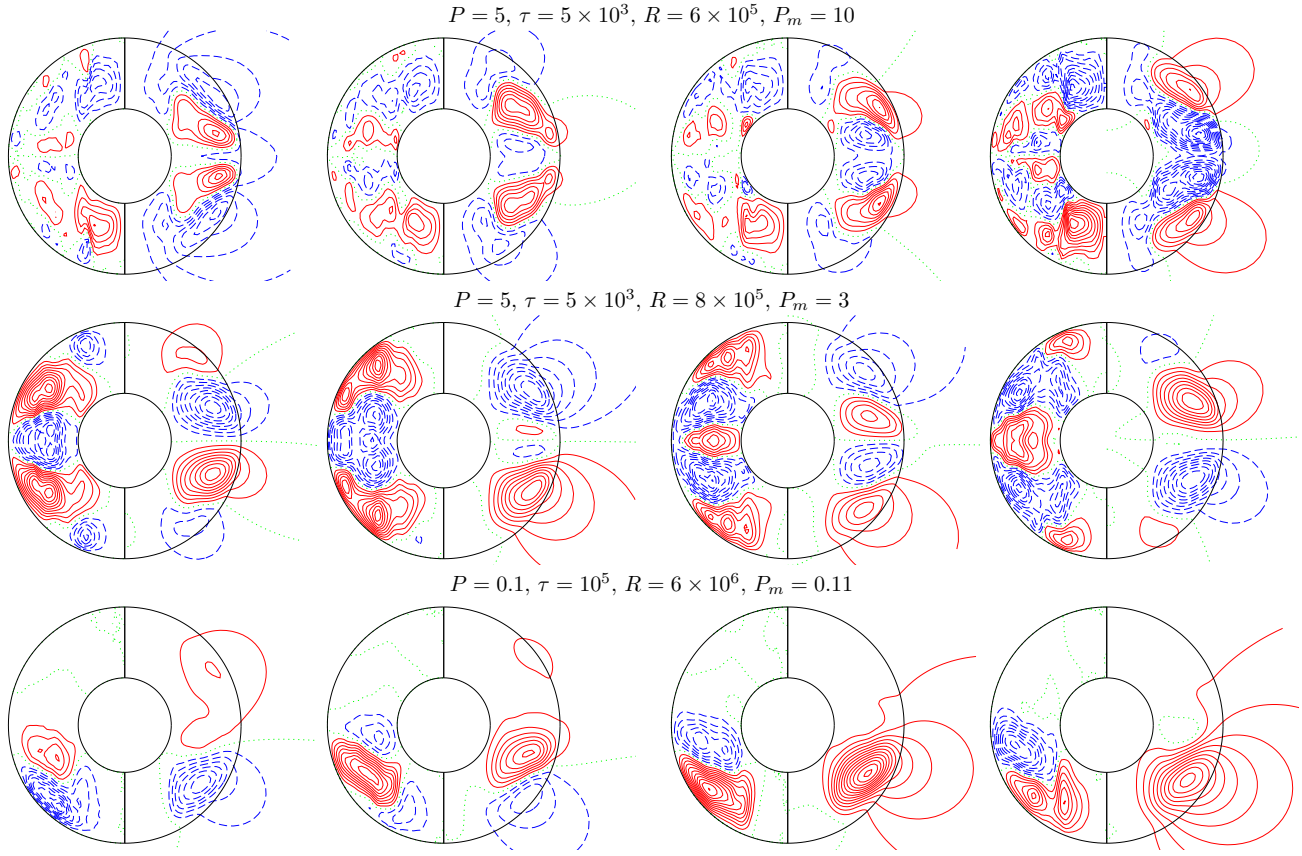

FIG. 9: *Plots for the last three cases of figure 8 at the times $n \cdot \Delta t$, $n = 3, 2, 1, 0$ (left to right) before the times of figure 8 with Δt =0.035,0.04,0.0025 (from top to bottom).*

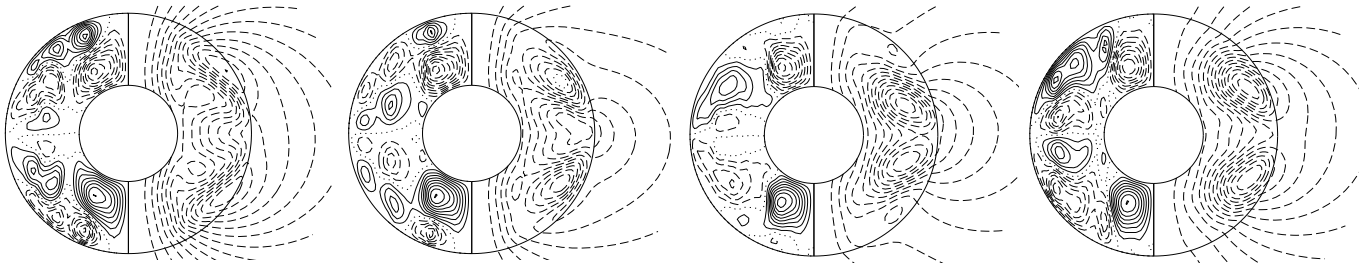

FIG. 10: *An "invisibly" oscillating dynamo with $\Delta t = 0.04$ in the case of $P = P_m = 5$, $\tau = 5 \times 10^3$ and $R = 6 \times 10^5$. The plots to the left show lines of constant $\overline{B_\varphi}$ in their left halves and meridional field lines, $r \sin\theta \partial_\theta \overline{h} = const.$, in their right halves.*

6. APPLICATIONS TO PLANETARY DYNAMOS

6.1 General Considerations

In many respects it is too early to model the dynamo process in particular planets. The numerical simulations of the kind discussed in the preceding sections are still rather removed from the parameter regime relevant to planetary interiors. Only most recently attempts have been made to extrapolate results to high Rayleigh numbers and high values of τ (Christensen and Aubert, 2006). Moreover, only the most important physical parameters have been taken into account and relevant properties such as compressibility and other deviations from the Boussi-

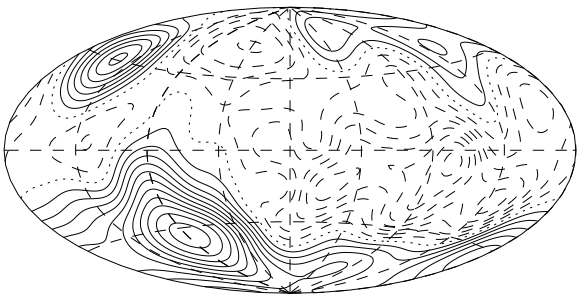

FIG. 11: *Lines of constant B_r at $r = r_o + 1$ for the dynamo with $R = 2 \times 10^6$, $\tau = 5 \times 10^3$, $P = P_m = 1$.*

nesq approximation have been considered only in special models applied to the Earth's core (Glatzmaier and Roberts 1996) or to the sun (Brun *et al.* 2004). On the other hand, many essential parameter values of planetary cores are not sufficiently well known to provide a basis for the development of specific dynamo models. Much of the future progress of the field will thus depend on the mutual constraints derived from observational evidence and from theoretical conclusions in order to arrive at a better understanding of the workings of planetary dynamos.

In table 2 some properties related to planetary magnetism have been listed. The dipole moments of the planets have been given as multiples of $G \cdot R_p^3$ where R_p denotes the mean radius of the planet or satellite. Thus the numerical value indicates the field strength in *Gauss* in the equatorial plane of the dipole at the distance R_p from its center. We have included Mars in the table, although it does have an active dynamo at the present time. The strong magnetization of the Martian crust indicates, however, that a strong field dynamo must have operated in the early history of the planet.

The most important question of the theory of planetary magnetism is the dependence of the observed field strength on the properties of the planet. We have already discussed in the historical introduction various proposals for such dependences based on *ad hoc* assumptions, but these have been abandoned by and large. Only the concept of an Elsasser number Λ of the order unity is still frequently used. Stevenson (2003) shows that a value $\Lambda = 0.3$ fits most of the planets with a global magnetic field quite well, but in cases such as Mercury and Saturn only a value of the order 10^{-2} can be estimated for Λ. In order to save the concept different dynamo regimes must be assumed. Equilibration balances for weaker magnetic fields have been proposed as, for instance, in the case when the strength of convection is not sufficient to attain the $\Lambda \sim 1$ balance. For details see Stevenson (1984).

An important balance often invoked in discussions of planetary dynamos (see, for example, Stevenson (1979) and Jones (2003)) is the MAC-balance (Braginsky 1967) where it is assumed that Lorentz force, buoyancy force and pressure gradient are all of the same order as the

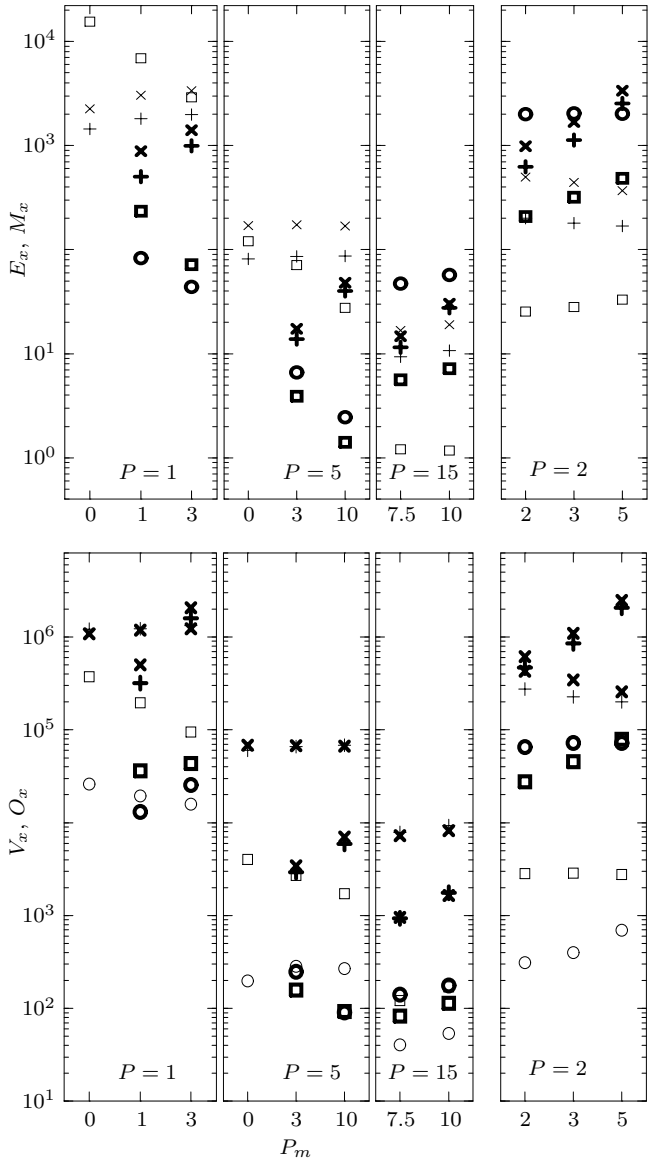

FIG. 12: *Kinetic E_x and magnetic M_x energy densities (upper part) and viscous V_x and Ohmic O_x dissipations (lower part) as functions of P_m for convection driven dynamos for $\tau = 5 \times 10^3$, $R = 10^6$ (left three columns), $\tau = 3 \times 10^4$, $R = 3.5 \times 10^6$ (right column) and Prandtl number as indicated in the boxes. The highest values of the Elsasser number for the cases $P = 1, 5, 15, 2$ are $\Lambda = 3.02$, 0.37, 0.49 and 1.12 respectively. The components $\overline{X}_p$, $\overline{X}_t$, $\check{X}_p$, $\check{X}_t$ (where $X = E, M, V, O$) are represented by circles, squares, plus-signs and crosses, respectively. Kinetic energy densities and viscous dissipations are shown with light symbols, magnetic energy densities and Ohmic dissipations are shown with heavy symbols. The magnetic Prandtl numbers $P_m = 0$ correspond to non-magnetic convection.*

Coriolis force, while viscous friction and the momentum advection term are regarded as negligible in the equations of motion. The neglection of the latter term is

Planet (Satellite)	Planetary Radius R_p (10^6 m)	Dipole Moment (10^{-4}T$\times R_p^3$)	Core Radius (10^6 m)	Angular Rate of Rot. Ω (10^{-5}s^1)	Magn. Diffus. (m^2/s)
Mercury	2.439	0.0025	1.9	0.124	~ 2
Earth	6.371	0.31	3.48	7.29	2
Mars	3.389	3†	~ 1.5	7.08	~ 2
Jupiter	69.95	4.3	56*	17.6	30*
Saturn	58.30	0.21	29*	16.2	4*
Uranus	25.36	0.23	18*	10.1	100*
Neptune	24.62	0.14	20*	10.8	100*
Ganymede	2.63	0.0072	0.7	1.02	4

* Since the Giant Planets do not possess a well-defined boundary of a highly conducting core, values of the most likely region of dynamo activity are given.
† Remnant magnetism of the Martian crust appears to require an ancient dynamo with a field strength of at least 10 times the Earth's magnetic field.

TABLE II: *Planetary parameter values (after Stevenson (2003), Nellis* et al. *(1988), Connerney (1993) and various websites).*

well justified for high Prandtl numbers, but it is doubtful for values of P of the order unity or less. Inspite of their smallness in comparison with the Coriolis force, the divergence of the Reynolds stress can generate the most easily excitable mode of a rotating fluid, namely the geostrophic differential rotation which can not be driven by the Coriolis force, the pressure gradient or buoyancy. Of course, an excitation by the Lorentz force is possible in principle. The latter force, however, usually inhibits the geostrophic differential rotation. Since the mean azimuthal component of the magnetic field is typically created through the shear of the differential rotation, the Lorentz force opposes the latter according to Lenz' rule.

Christensen and Aubert (2006) have recently introduced a concept in which the equilibrium strength of planetary magnetism does no longer depend on the rate of rotation Ω, but instead depends only on the available power for driving the dynamo. They find that scaling laws can be obtained once Rayleigh number, Nusselt number and dimensionless buoyancy flux $\hat{Q}$ have been defined through quantities that no longer involve molecular diffusivities. This is a surprising result since it requires the presence of rotation and can not be achieved in a non-rotating system. The final estimate obtained for the strength of the magnetic field in the dynamo region fits the cases of the Earth and Jupiter quite well, but yields the result that Mercury's field could not be generated by a buoyancy driven dynamo since the magnetic Reynolds number would be too small. In the cases of the outer planets relevant parameters are not sufficiently well known to draw definitive conclusions.

Finally we like to draw attention to what has been called Stevenson's paradox, namely that a too high electrical conductivity is detrimental for dynamo action in planetary cores. According to the Wiedemann-Franz law

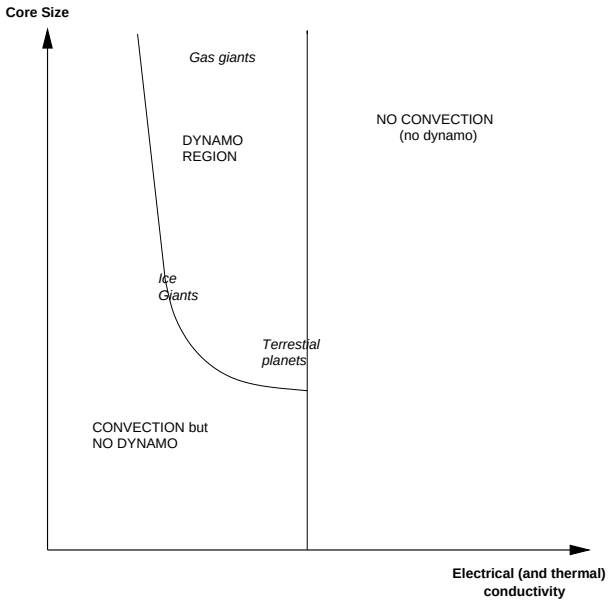

FIG. 13: *Sketch of Stevenson's paradox (after Stevenson 2003).*

of condensed matter physics the thermal conductivity k of a metal is proportional to its electrical conductivity times the temperature, $k = \sigma TL$, where L has approximately the same value for all metals. This is due to the fact that in metals electrons dominate both, the transports of heat and of charge. As a consequence there is an upper bound on the electrical conductivity for which a dynamo driven by thermal convection is possible because a high value of σ implies a low temperature change with increasing depth needed to carry the heat from the interior of the planetary core. But as soon as the temperature change with pressure falls below its isentropic value

thermal convection disappears and a stably stratified environment is obtained which makes it difficult to drive a dynamo by other types of motions such as compositional convection. Ignoring the latter possibility Stevenson (2003) has sketched the diagram shown in figure 13 where the marginal nature of dynamos in terrestrial as well as in the "icy" planets is indicated.

In the following brief characterizations of the magnetisms of various planets and moons are given. In terrestrial planets and satellites dynamos are possible in the liquid parts of their iron cores. Such cores always include light elements which depress the temperature of freezing and can give rise to compositional buoyancy in the presence of a solidifying inner part of the core. In Jupiter and especially in Saturn convection may also be driven in part by compositional buoyancy since hydrogen and helium are immiscible in certain regions and helium drops may rain out. In numerical dynamo models the different sources of buoyancy are usually not distinguished, however.

6.2 Mercury

It has already become apparent that the origin of Mercury's magnetism is especially enigmatic. Besides the hypothesis of an active dynamo, thermoelectric currents and remnant magnetism of the crust compete as explanations. The latter possibility had been discarded for a long time since Runcorn's theorem states that a homogeneous spherical shell can not be magnetized by an interior magnetic field in such a way that a dipolar field can be observed from the outside after the interior source has been removed (Runcorn, 1975). Aharonson et al. (2004) have shown, however, that plausible inhomogeneities of the crust could possibly explain a remnant magnetic field created by an ancient dynamo.

The idea that a convection driven dynamo operates in a fluid outer core of Mercury has received some support from observations of Mercury's librations (Margot et al., 2004) and from numerical simulations (Stanley et al., 2005). The amplitudes of the small periodic variations (librations) of Mercury's rotation caused by the gravitational pull of the sun on the non-axisymmetric mass distribution of Mercury appear to be too large for a fully solidified planet. This suggests that the solid inner core is separated from the mantle by a fluid outer core in which convection flows may occur. The numerical simulations of dynamos in the thin shell of the outer core have demonstrated that the dipole strength measured from the outside may not be representative for the strength of the magnetic field at the core-mantle boundary and the criteria mentioned above may be satisfied after all. The question, however, whether there is a sufficiently strong source of buoyancy to sustain convection and the dynamo over the age of the planet has not yet been answered satisfactorily.

6.3 Venus

Space probes have clearly shown that there is no dynamo operating presently in Venus. This result is surprising since Venus is very similar to the Earth in many other aspects. That the period of rotation is only 1/243 of a day should not matter much since the Coriolis parameter τ is still huge. More important is the fact that the cooling of the planet is less efficient because of the apparent absence of mantle convection and plate tectonics. A solid inner core may not have yet started to grow in Venus and vigorous convection does not occur in the core, at least not at the present time.

6.4 Mars and Moon

Neither Moon nor Mars have an active dynamo, but the magnetized rocks in their crusts suggest that in their early history about 4 billion years ago dynamos may have been operating in the iron cores of these bodies. The small lunar core with a radius of the order of 350 km and the age of the magnetized lunar rocks put severe constraints on a possible dynamo origin of lunar magnetism as discussed by Stegman et al. (2003). In their model these authors try to accommodate in particular the apparent sudden onset of a lunar dynamo at a time $3.5\,Ga$ ago. Because of its larger iron core the possibility of a temporarily operating Martian dynamo is more likely, but the strong magnetization of parts of the Martian crust requires a field of at least ten times the strength of the present geomagnetic field. For a recent review of the implications of Martian magnetism for the evolution of the planet we refer to Stevenson (2001).

6.5 Jupiter

The Jovian magnetic field is rather similar to the geomagnetic one sharing with it a dipole axis that is inclined by an angle of the order of 10 degrees with respect to the axis of rotation. That the higher harmonics of the field are relatively stronger than those in the case of the Earth suggest that the Jovian dynamo is driven at a more shallow layer than the Earth's outer core. This assumption is in accordance with the transition to metallic hydrogen which is expected to occur at a pressure of $140GPa$ corresponding to a region with a radius of 0.9 of the Jovian radius (Nellis et al., 1996). The transition is not a sharp one as suggested by earlier models of Jupiter's interior, but a gradual one leading to a decrease of the magnetic diffusivity down to about $4m^2/s$. Since this value yields

a rather high value for the Elsasser number Λ Stevenson (2003) has argued that the dynamo is most active above the region of highest conductivity. Jones (2003), on the other hand, accepts the value 20 for Λ, but must admit a high magnetic Reynolds number of the order 10^4 at which an effective dynamo may no longer be possible. A detailed model of a convection driven Jovian dynamo should include effects of compressibility and depth dependent electrical conductivity, but none has yet been published.

6.6 Saturn

Saturn's magnetic field with a strength of $0.2mT$ near the poles is much weaker than that of Jupiter which must be attributed primarily to its deeper origin in the planet. The transition pressure of $140GPa$ is reached only at about half the planetary radius. A property that has received much attention is that the Saturnian magnetic field is nearly axisymmetric with respect to the axis of rotation. This property can not be interpreted as a contradiction to Cowling's (1934) theorem since it has long been shown that fields with arbitrarily small deviations from axisymmetry can be generated by the dynamo process (Braginsky 1976). Stevenson (1982) gave a reasonable explanation for the almost axisymmetric Saturnian field by demonstrating that the differential rotation in the stably stratified, but still electrically conducting gas shells above the dynamo region will tend to shear off all non-axisymmetric components of the field. The problem may be a bit more intricate as has been pointed out by Love (2000) who showed that sometimes fields with solely non-axisymmetric components are found in such situations.

6.7 Uranus and Neptune

A metallic liquid probably does not exist in Uranus and Neptune whose interiors consist mostly of ice and rocks. Because of the pressure dissociation of water deeper regions of these planets are characterized by an ionic conductivity which is lower than typical metallic conductivities by between one and two orders of magnitude. The mixture of water, methane, ammonia and other ices is sufficiently fluid that convection can occur and that a dynamo is thus possible. The fact that the observed magnetic field do not show an alignment with the axis planetary rotation and that quadrupolar and octupolar components are comparable to the dipolar components of the fields has been attributed to a dynamo operating in a thin shell (Ruzmaikin and Starchenko, 1991; Stanley and Bloxham, 2004). This seems be hardly necessary, however, since even convection driven dynamos in thick shells often exhibit such fields when small scale components dominate as in the case of high Rayleigh numbers and low Prandtl numbers. See, for example, figure 11 which shows a magnetic field rather similar to that of Uranus as displayed in the paper of Connerney (1993). A special difficulty for a convection driven dynamo in the interior of Uranus is caused by its low emission of heat. Holme and Bloxham (1996) suggest that a typical dynamo would involve more Ohmic dissipation than corresponds to the heat flux emitted from the interior of the planet.

6.8 Ganymede and other Satellites

It came as a great surprise when the measurements of the Galileo spacecraft indicated that Jupiter's moon Ganymede possesses a global magnetic field for which an active dynamo inside the satellite seems to be the only realistic explanation (Kivelson et al., 1996), although the possibility of a remnant magnetism can not easily be excluded (Crary and Bagenal 1998). It must be kept in mind that Ganymede is the largest satellite in the solar system which exceeds even Mercury in size. Nevertheless the estimated radius of its iron core is only about 660 km and it is hard believe that it could still be partly molten unless it contain a lot of radioactive potassium 40 or Ganymede was captured into a resonance in its more recent history (Showman *et al.* 1997). The fact that Ganymede's magnetic moment is nearly aligned with the ambient Jovian magnetic has led to the suggestion that the ambient field could aid significantly Ganymede's dynamo. Sarson et al. (1997) have investigated this question with the result that the ambient field is too weak to exert much influence. On the other hand, in the case of Io which is much closer to Jupiter the interaction between the ambient field and the liquid iron core can explain the observed structure of the magnetic field without the assumption of an active dynamo.

There are no other satellites in the solar system where an active dynamo must be suspected. The substantial magnetization of many iron meteorites suggest, however, that several differentiated proto-planets have had dynamos in the early days of the solar system.

7. CONCLUDING REMARKS

It is apparent from the above discussions that dynamo theory does not yet have much specific information to contribute to the interpretation of the observed magnetic properties of planets and satellites in the solar system. Even possible interactions between thermal and compositional buoyancies have not yet been taken fully into account (Glatzmaier and Roberts 1996, Busse 2002b). Some typical properties are already apparent, however, as for instance:

- Dynamos that are dominated by a nearly axial dipole and exhibit a magnetic energy that exceeds the kinetic one by orders of magnitude as in the case of the Earth are typical for high effective Prandtl numbers as must be expected when convection is primarily driven by compositional buoyancy. The rather Earth like appearance of the dynamo of Glatzmaier and Roberts (1995) is in part due to the high value of P used in their computational model.
- Dynamos exhibiting strong higher harmonics are more likely driven by thermal convection corresponding to Prandtl numbers of the order unity or less.
- Dynamo oscillations are a likely phenomenon in the presence of a sufficiently strong differential rotation. They may not always be apparent in the poloidal magnetic field seen at a distance from the dynamo region.
- Considerations based on the effects on convection of an imposed homogeneous magnetic field can not directly be applied to the case of convection driven dynamos.

More details on the parameter dependence of dynamos will certainly emerge in the future as the increasingly available computer capacity will allow extensions of the parameter space accessible to computer simulations. Space probes such as MESSENGER in the case of Mercury will provide much needed detailed information on planetary magnetic fields. Eventually we may learn more about their variation in time which is one of the most interesting properties of planetary magnetic fields.

As in the case of stellar magnetism where the study of star spots and stellar magnetic cycles is contributing to the understanding of solar magnetism it may eventually become possible to learn about the magnetism of extrasolar planets and apply this knowledge for an improved understanding of solar system dynamos. Undoubtedly the field of planetary magnetism will continue to be an exciting one!

8. References

Aharonson O, Zuber M T, Solomon S C 2004 Crustal remanence in an internally magnetized non-uniform shell: a possible source for Mercury's magnetic field? *Earth Plan. Sci. Lett.* **218** 261-268

Ardes M, Busse F H, Wicht J 1997 Thermal convection in rotating spherical shells. *Phys. Earth Plan. Int.*, **99**, 55-67

Backus G 1958 A class of Self-Sustaining Dissipative Spherical Dynamos. *Annals Phys.* 4, 372-447

Braginsky S I 1967 Magnetic waves in the earth's core. *Geomagn. Aeron.*, **7**, 851-859

Braginsky S I 1976 On the nearly axially-symmetrical model of the hydromagnetic dynamo of the Earth. *Phys. Earth Plan. Int.*, **11**, 191-199

Brun A S, Miesch M S, Toomre J 2004 Global-Scale Turbulent Convection and Magnetic Dynamo Action in the Solar Envelope. *Astrophys. J.* **614**, 1073-1098

Bullard E C 1949 The magnetic field within the earth. *Proc. Roy. Soc. London*, **A 197**, 433-463

Burke B F, Franklin K L 1955 Observations of variable radio source associated with the planet Jupiter. *J. Geophys. Res.*, **60**, 213-217

Busse F H 1976 Generation of Planetary Magnetism by Convection. *Phys. Earth Plan. Inter.*, **12**, 350-358

Busse F H 1983 Recent developments in the dynamo theory of planetary magnetism, *Ann. Rev. Earth Plan. Sci.* **11**, 241-268

Busse F H 2002a Convection flows in rapidly rotating spheres and their dynamo action. *Phys. Fluids*, **14**, 1301-1314

Busse F H 2002b Is low Rayleigh number convection possible in the Earth's core? *Geophys. Res. Letts.*, **29**, GLO149597

Busse F H, Carrigan C R 1976 Laboratory simulation of thermal convection in rotating planets and stars, *SCIENCE*, **191**, 81-83

Busse F H, Cuong P G 1977 Convection in rapidly rotating spherical fluid shells. *Geophys. Astrophys. Fluid Dyn.* **8**, 17–41

Busse F H, Grote E, Simitev R 2003 Convection in rotating spherical shells and its dynamo action, pp. 130-152 *in "Earth's Core and Lower Mantle", C.A.Jones, A.M.Soward and K.Zhang, eds., Taylor & Francis*

Busse F H, Heikes K E 1980 Convection in a Rotating Layer: A Simple Case of Turbulence, *SCIENCE*, **208**, 173-175

Busse F H, Simitev R 2004 Inertial convection in rotating fluid spheres. *J. Fluid Mech.* **498**, 23–30.

Christensen U R, Aubert J 2006 Scaling laws for dynamos in rotating spherical shells. *Geophys. J. Int.*, in press

Christensen U R, Aubert J, Cardin P, Dormy E, Gibbons S, Glatzmaier G A, Grote E, Honkura Y, Jones C, Kono M, Matsushima M, Sakuraba A,

Takahashi F, Tilgner A, Wicht J, Zhang K 2001 A numerical dynamo benchmark. *Phys. Earth Plan. Inter.*, **128**, 25-34

Christensen U, Olson P, Glatzmaier, G A 1999 Numerical Modeling of the Geodynamo: A Systematic Parameter Study. *Geophys. J. Int.*, **138**, 393–409.

Chandrasekhar S 1961 *Hydrodynamic and Hydromagnetic Stability*, Clarendon Press, Oxford

Childress S, Soward A M 1972 Convection-driven hydrodynamic dynamo *Phys. Rev. Lett.* **29**, 837-839

Connerney J E P 1993 Magnetic Fields of the Outer Planets. *J. Geophys. Res.* **98**, 18659-18679

Crary F J, Bagenal F 1998 Remanent ferromagnetism and the interior structure of Ganymede.*J. Geophys. Res.* **103**, 25757-25773

Dolginov Sh Sh 1977 Planetary Magnetism: A Survey *Geomagn. Aeron.*, **17**, 391-406

Cowling T G 1934 The magnetic field of sunspots. *Monthly Not. Roy. astr. Soc.***34**, 39-48

Fearn D R 1979 Thermal and magnetic instabilities in a rapidly rotating fluid sphere. *Geophys. Astrophys. Fluid Dyn.*, **14**, 103–126

Giampieri G, Balogh A 2002 Mercury's thermoelectric dynamo model revisited. *Planet. Space Sci.*, **50**, 757-762

Gilbert N 1600 *De Magnete, Gilbert Club revised English translation*, Chiswick Press, London

Glatzmaier G A, Roberts P H 1995 A three-dimensional self-consistent computer simulation of a geomagnetic field reversal. *Nature* **377**, 203-209

Glatzmaier G A, Roberts P H 1996 An anelastic evolutionary geodynamo simulation driven by compositional and thermal convection. *Physica D* **97**, 81-94

Grote E, Busse F H 2001 Dynamics of convection and dynamos in rotating spherical fluid shells. *Fluid Dyn. Res.*, **28**, 349-368

Grote E, Busse F H, Tilgner A 2000 Regular and chaotic spherical dynamos. *Phys. Earth Planet. Inter.* **117**, 259-272

Herzenberg A 1958 Geomagnetic Dynamos. *Phil. Trans. Roy. Soc. London* **A250**, 543-585

Hide R 1974 Jupiter and Saturn. *Proc. Roy. Soc. London* **A 336**, 63-84

Holme R, Bloxham J 1996 The magnetic fields of Uranus and Neptun: Methods and models. *J. Geophys. Res.* **101**, 2177-2200

Jacobs J A 1979 Planetary Magnetic Fields. *Geophys. Res. Letts.*, **6**, 213-214

Jones C A 2000 Convection-driven geodynamo models. *Phil. Trans. Roy. Soc. London* **A358**, 873-897

Jones C A 2003 Dynamos in planets. In: Thompson M J, Christensen-Daalsgard J. (eds.) *Stellar Astrophysical Fluid Dynamics* Cambridge University Press, pp. 159-176

Jones C A, Soward A M, Mussa A I 2000 The onset of thermal convection in a rapidly rotating sphere. *J. Fluid Mech.* **405**, 157-179

Kivelson M G, Khurana K K, Russell C T, Walker R J, Warnecke J, Coroniti F V, Polanskey C, Southwood D J, Schubert G 1996 Discovery of Ganymede's magnetic field by the Galileo spacecraft. *Nature* **384**, 537-541

Kutzner C, Christensen, U R 2000 Effects of driving mechanisms in geodynamo models. *Geophys. Res. Lett.* **27** 29–32.

Kutzner K, Christensen U 2002 From stable dipolar towards reversing numerical dynamos. *Phys. Earth Planet. Inter.*, **131**, 29-45

Larmor J 1919 How could a rotating body such as the sun become a magnet? *Brit. Ass. Advan. Sci. Rep.* 159-160

Love J J 2000 Dynamo action and the nearly axisymmetric magnetic field of Saturn. *Geophys. Res. Letts.*, **27**, 2889-2892

Malkus W V R 1994 Energy Sources for Planetary Dynamos. In: Proctor M R E, Gilbert A D (eds.) *Lectures on Planetary and Solar Dynamos* Cambridge University Press, pp. 161-179

Malkus W V R 1968 Precession of the Earth as the Cause of Geomagnetism. *SCIENCE* **160** 259-264

Margot J, Peale S, Jurgens R F, Slade M A, Holin I V 2004 Earth-based measurements of Mercury's forced librations in longitude. *Eos Trans. AGU* **85** GP33-03

Nellis W J, Hamilton D C, Holmes N C, Radousky H B, Ree F H, Mitchell A C, and Nicol M 1988 The Nature of the Interior of Uranus Based on Studies of Planetary Ices at High Dynamic Pressure. *SCIENCE*, **240**, 779-781

Nellis W J, Weir S T, and Mitchell A C 1996 Metallization and Electrical Conductivity of Hydrogen in Jupiter. *SCIENCE*, **273**, 936-938

Runcorn S 1975 An ancient lunar magnetic field. *Nature* **253** 701-703

Ruzmaikin A A, Starchenko S V 1991 On the origin of Uranus and Neptune magnetic fields. *Icarus*, **93**, 82-87

Sarson G R, Jones C A, Zhang K, Schubert G 1997 Magnetoconvection dynamos and the magnetic field of Io and Ganymede. *SCIENCE*, **276**, 1106-1108

Showman A P, Stevenson D J, Malhotra R 1997 Coupled orbital and thermal evolution of Ganymede. *Icarus* **129**, 367-383

Simitev R, Busse F H 2005 Prandtl-number dependence of convection-driven dynamos in rotating spherical fluid shells. *J. Fluid Mech.* **532**, 365-388

Somerville R C J, Lipps F B 1973 A Numerical Study in Three Space Dimensions of Bénard Convection in a rotating Fluid. *J. Atmos. Sci.* **30**, 590-596

Soward A M 1974 A convection driven dynamo, I, The weak field case. *Phil. Trans. Roy. Soc. London* **A275**, 611-645

Stanley S, Bloxham J, Hutchison W E, and Zuber M T 2005 Thin shell dynamo models consistent with Mercury's weak observed magnetic field. *Earth Plan. Sci. Lett.* **234** 27-38

Stegman D R, Jellinek A M, Zatman S A, Baumgardner J R and Richards M A 2003 An early lunar core dynamo driven by thermochemical mantle convection. *Nature* **421** 143-146

Stevenson D J 1979 Turbulent Thermal Convection in the Presence of Rotation and a Magnetic Field. *Geophys. Astrophys. Fluid Dyn.*, **12**, 139-169

Stevenson D J 1982 Reducing the non-axisymmetry of a planetary dynamo and an application to Saturn. *Geophys. Astrophys. Fluid Dyn.*, **21**, 113-127

Stevenson D J 1983 Planetary magnetic fields. *Rep. Prog. Phys.* **46**, 555-620

Stevenson D J 1984 The Energy Flux Number and Three Types of Planetary Dynamo. *Astron. Nachr.* **305**, 257-264

Stevenson D J 1987 Mercury's magnetic field: a thermoelectric dynamo? *Earth Planet. Sci. Lett.* **82**, 114-

Stevenson D J 2001 Mars' core and magnetism. *Nature* **412** 214-219

Stevenson D J 2003 Planetary magnetic fields. *Earth Planet. Sci. Lett.* **208**, 1-11

Tilgner A 1999 Spectral Methods for the Simulation of Incompressible Flows in Spherical Shells. *Int. J. Numer. Meth. Fluids*, **30**, 713-724

Tilgner A 2005 Precession driven dynamos. *Phys. Fluids*, **17**, 034104-1-6

Tilgner A, Busse F H 1997 Finite amplitude convection in rotating spherical fluid shells, *J. Fluid Mech.*, **332**, 359-376

Vanyo J P 1984 Earth core motions: experiments with spheroids. *Geophys. J. Roy. astr. Soc.* **77**, 173-183

Zhang K 1994 On coupling between the Poincaré equation and the heat equation. *J. Fluid Mech.*, **268**, 211-229

Zhang K 1995 On coupling between the Poincaré equation and the heat equation: no-slip boundary condition. *J. Fluid Mech.*, **284**, 239-256